

An *ab initio* molecular dynamics study of varied compositions of the LiF-NaF-KF molten salt

Veronica Heyl^a, Benjamin Beeler^{a,b}

^a*North Carolina State University, Raleigh, 27607, NC, USA*

^b*Idaho National Laboratory, Idaho Falls, 83415, ID, USA*

Abstract

With increasing interest in molten salt reactors, there becomes a demand for investigations into thermophysical properties of salt systems. The LiF-NaF-KF (FLiNaK) salt system is a primary candidate for use in these reactors. However, the thermophysical properties of compositions outside the eutectic composition are still largely unknown. In this article, properties of ten unique compositions, including four ternary compositions, are investigated using *ab initio* molecular dynamics simulations across five temperatures between 900 K and 1300 K. The properties of interest are the density, thermal expansion, bulk modulus, compressibility, heat capacity, and enthalpy of mixing. In general, the results were found to be in good agreement with other literature and experimental results. The density and heat capacity had a tendency to be slightly underpredicted. No conclusions could be drawn about the bulk modulus and compressibility in terms of compositional dependence. The thermal expansion had a negative trend with respect to the LiF concentration and no trends were observed for the NaF or KF concentration. The enthalpy of mixing shows minima for the ternary compositions, with the near-equiautomic composition exhibiting the lowest values. This work shows the potential for compositional tailoring in the FLiNaK system to optimize thermophysical properties.

Keywords: molten salts, thermophysical properties, AIMD, FLiNaK

1. Introduction

Molten salts are ionic liquid mixtures at high temperatures with high heat capacity and thermal conductivity. These properties make molten salts useful as a coolant or fuel salt for molten salt reactors (MSRs). Research into MSRs was largely neglected after the experiments by Oak Ridge National Laboratory during the late 1960s[1]. The advantages of an MSR compared to solid fuel reactors are that MSRs do not need traditional fuel fabrication, possess increased intrinsic safety, and have a high working temperature[2]. Because of their benefits, there has been renewed interest in MSRs in the past few years. With this comes the need to characterize molten salts and determine their thermophysical properties, which are required to parameterize complex fluid dynamics and chemical interaction models[1, 3].

The LiF-NaF-KF (FLiNaK) salt system is one of the primary candidates to operate as a coolant salt in MSRs. FLiNaK has been proposed as the heat transfer medium in the Very High-Temperature Reactor, a graphite-moderated, gas-cooled Generation IV concept reactor[4], and is of interest to serve as the primary coolant in MSRE-type designs. FLiNaK

is also often utilized as a surrogate for LiF-BeF₂ (FLiBe), which is also of interest in MSRs, but more challenging to explore experimentally due to the toxicity of Be. The volumetric heat capacity for FLiNaK is similar to water but without the issue of critical heat flux due to the large margin to boiling. Additionally, FLiNaK can operate under ambient pressure conditions, allowing for the removal of the high system pressure in water-cooled reactors [5]. Thus, a significant amount of experimental research has been performed on FLiNaK to determine select thermophysical and chemical properties.

Frandsen et al. investigated the density as a function of temperature between approximately 500°C and 1500°C, the total scattering structure function, and the pair distribution function of the eutectic composition[6]. Anderson et al. collaborated with Oak Ridge National Laboratory to determine the density, equilibrium volume, coefficient of thermal expansion, self-diffusion coefficients for constituent ions at 973 K, 1223 K, and 1423 K, and the self-diffusion coefficient for solute ions at 973 K[7]. All of these properties were determined at the eutectic composition. Liu et al. studied the microstructures of lutetium fluoride and oxyfluoride structures in eutectic FLiNaK using Raman spectroscopy and density functional theory[8]. Ambrosek et al. used previously acquired experimental data to determine the heat transfer of the eutectic composition in comparison to the Dittus-Boelter correlation[5]. Additional experiments have been performed on the eutectic composition [9, 10, 11].

Thermophysical properties are difficult to determine experimentally because of the toxicity of salts, the targeted high temperatures, and the cost of the experiment [1]. In lieu of an abundance of high-fidelity experimental data, a computational approach can be pursued to complement and supplement the existing experimental data. Salanne et al. constructed interatomic potentials for mixtures of LiF, NaK, KF, and ZrF₄ and used them for molecular dynamics simulations to evaluate the heat-transfer properties of FLiNaK and NaF-ZrF₄[12]. Lee et al. used molecular dynamics to train neural network forcefields and reparametrized analytical forcefields in order to use large-scale molecular dynamics in the determination of structural and transport properties[13]. Sona et al. used computational fluid dynamics simulations to investigate the flow and heat transfer characteristics of eutectic FLiNaK[14]. Recently, *ab initio* molecular dynamics simulations (AIMD) have begun to be explored to determine thermophysical properties, structure, and speciation in FLiNaK[15, 6, 16, 17].

The common trend among previous works is the selection of investigating only the eutectic composition. As most experimental work has been done on this composition, previous computational work purposely and appropriately chose to focus on the composition that had data available for comparison. While understandable, due to corrosion, changing redox potential, and other variables in a reactor environment, the composition of the salt may slightly change as a function of time. Additionally, while the eutectic composition has the minimum melting point for this ternary system, there may be other properties (density, viscosity, heat capacity, etc.) that are more beneficial at non-eutectic compositions, but which are largely unknown[4].

This work seeks to more fully characterize the thermophysical properties of FLiNaK through a first principles computational investigation of four ternary compositions (including the eutectic), three binary eutectic compositions, and three pure alkali-halide salt constituents. The density, bulk modulus, compressibility, heat capacity, thermal expansion, and enthalpy of mixing for each different composition in the FLiNaK system will be determined using appropriate temperatures between 900 K and 1300 K. This is the most extensive in-

60 investigation of thermophysical properties across the compositional and temperature regimes
61 in the nuclear-relevant molten salt FLiNaK.

62 **2. Computational Methods**

63 Ten unique compositions (all compositions are stated in mole percent) were studied for
64 the LiF-NaF-KF salt system, including four ternary compositions (eutectic 46-12-42, 16-
65 42-42, 32-34-34, and 42-42-16), three binary eutectic compositions (0-40-60, 51-0-49, and
66 61-39-0), and the three pure alkali-halide salt constituents (LiF, NaF, and KF). The initial
67 structure was prepared by inserting the respective molecules into a supercell via the Packmol
68 package [18], with 100 atoms for the ternary systems and 200 atoms for all other systems.
69 Such system sizes have been shown to produce converged and comparable results for AIMD
70 analyses of molten salts [19, 20]. AIMD simulations were performed using the Vienna *ab*
71 *initio* Simulation Package (VASP)[21, 22, 23]. The temperature range investigated for each
72 composition depended upon the corresponding melting point of that composition, with the
73 ternary system temperatures ranging from 900 K to 1300 K, binary system temperatures
74 from 1000 K to 1300 K, and the pure constituent temperatures from 1100 K to 1300 K. The
75 energy cutoff was 600 eV, which is 100 eV higher than the recommended maximum for the
76 pseudopotentials utilized, and the electronic optimization criterion was 10^{-3} eV. Convergence
77 testing was performed with more fine energy convergence criteria to ensure that the results
78 were not affected by the choice of electronic optimization. A $1 \times 1 \times 1$ k-point mesh was used,
79 as this has been shown to be sufficient in prior simulations for molten salts with similarly
80 sized supercells[24, 15]. The vdW-DF2 van der Waals functional was used to account for the
81 dispersion interactions[25, 26]. While there are many choices of dispersion interactions avail-
82 able within VASP, this specific choice was made due to its ability to replicate the properties
83 of various chloride salts[24]. A brief examination of the DFT-D3 dispersion correction term
84 [27] was also explored, which did not show superior predictions.

85 In the Open Visualization Tool (OVITO)[28], the initial structures were verified to have
86 no bonds shorter than 1.5 Å, indicating a reasonable initial guess. The structures were
87 equilibrated using VASP at each temperature studied. The initial equilibrium simulation for
88 each composition occurred at 1100 K. The energy was evaluated versus time to check if the
89 system was equilibrated. If the slope of the running average was approximately zero, the
90 structure was considered to be at equilibrium. If not, the simulation was continued until it
91 was determined that equilibrium was reached. Typically, equilibration takes approximately
92 10-15 ps.

93 Utilizing the equilibrated structures, the system was further evolved at different specified
94 volumes to obtain the pressure as a function of volume. The systems were equilibrated for a
95 further 4 ps, with time-averaging to determine the energy and pressure over the final 3 ps.
96 At least six data points were included for each composition and temperature, ensuring that
97 the pressures ranged from -2 to +10 kbar, with at least one pressure greater than 5 kbar.
98 This is in accordance with a prior procedure utilized[24]. Five simulations were performed
99 for each unique volume for statistical significance. Thus, for a given composition and tem-
100 perature, approximately thirty simulations were performed. The pressure as a function of
101 the volume, shown in fig. 1a, was determined by fitting a quadratic equation, allowing for
102 the determination of the volume at which the pressure is zero.

103 The zero pressure volume, along with the mass, was used to calculate the density. The
 104 parabolic fit of the volume-pressure curve was used to calculate the bulk modulus and com-
 105 pressibility:

$$K = -V \left(\frac{\partial P}{\partial V} \right)_{P=0} = \frac{1}{\beta} \quad (1)$$

106 where K is the bulk modulus, V is the volume, P is the pressure, and β is the compressibility.

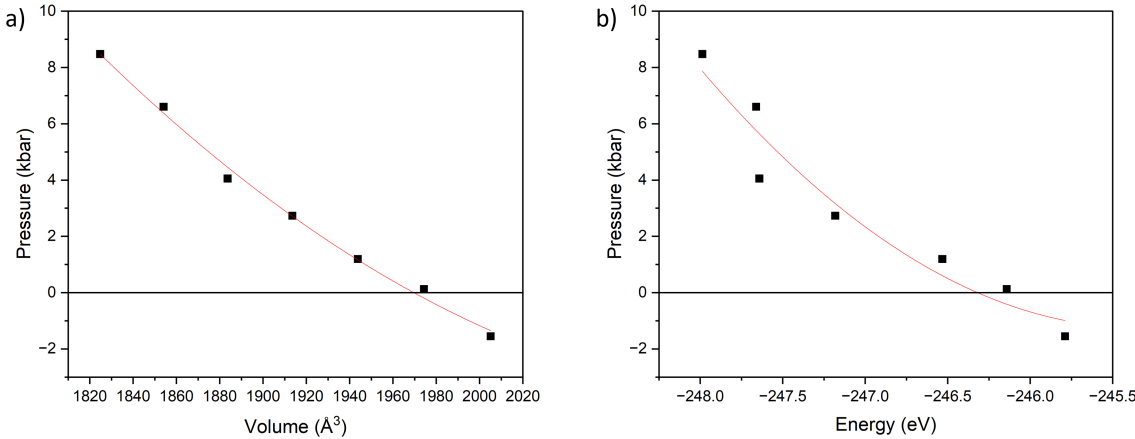


Figure 1: An example of the a) pressure as a function of volume and b) pressure as a function of energy for the 16-42-42 mol% composition at 1000 K.

107 In a similar manner used to determine the density, the heat capacity can also be found.
 108 The pressure as a function of potential energy, shown in fig. 1b, was determined by fitting
 109 a quadratic equation, allowing for the determination of the potential energy at which the
 110 pressure is zero. This zero-pressure potential energy is then added to the kinetic energy,
 111 and the total energy is plotted versus temperature. A linear function is fit to the data to
 112 obtain the total energy as a function of temperature. From this, the heat capacity can be
 113 determined:

$$C_p = \lim_{\Delta T \rightarrow 0} \frac{\partial E}{\partial T} \quad (2)$$

114 where C_p is the heat capacity, T is the absolute temperature, and E is the total energy. It
 115 was verified that a linear function adequately represented the data, indicating a constant
 116 heat capacity over the temperature range investigated.

117 The thermal expansion is determined by analyzing the zero-pressure volume as a function
 118 of temperature, treating the coefficient of thermal expansion (α) as:

$$\alpha = \frac{1}{V_0} \left(\frac{\partial V}{\partial T} \right)_p \quad (3)$$

119 where V_0 is a reference volume at the lowest temperature explored for each composition.

120 The enthalpy of mixing is determined from the potential energy of the mixed system and
 121 the three binary salts:

$$\Delta H^{mix} = \frac{E_{ABC}}{M_{ABC}} - \frac{x_A E_A}{M_A} - \frac{x_B E_B}{M_B} - \frac{x_C E_C}{M_C} \quad (4)$$

122 where M_i is the number of molecules in the system, E_A , E_B , and E_C are the potential energies
 123 of the reference systems (LiF, NaF, and KF), E_{ABC} is the potential energy of the ternary
 124 system, and x_A , x_B , and x_C are the mole fraction of the respective reference salts in the
 125 mixture. This same equation can be applied to binary salt mixtures, reducing from four
 126 terms to three. While assumptions can be made to incorporate entropic effects to determine
 127 the free energy of mixing, such a step was not taken due to inherent assumptions required
 128 for ideal solution-type behavior.

129 The binary and unary salt systems were equilibrated in a strictly NPT ensemble, easing
 130 some of the computational burden of exploring varied salt complexes, but limiting the ability
 131 to explore volume-dependent phenomena, such as the compressibility. There are no statis-
 132 tically significant differences in calculated thermodynamic quantities from the utilization of
 133 an NPT versus an NVT ensemble.

134 3. Results

135 3.1. Density and Thermal Expansion

136 The density of each composition studied is displayed as a function of temperature in fig. 2.
 137 It should be noted that for all densities reported here, there is an approximate error of 0.05
 138 g/cc. For all compositions, the density decreases with increasing temperature. This is in line
 139 with the inversely proportional relationship between density and temperature. The minimum
 140 density is observed for the pure LiF system, while the maximum density is observed for the
 141 NaF system. All of the densities fall within a range of approximately 0.25 g/cc, with the
 142 intermediate compositions having a much narrower range of only about 0.1 g/cc. Thus, the
 143 maximum variation for the ternary compositions is approximately 5%. All data presented is
 144 also included in tabular form in the appendix.

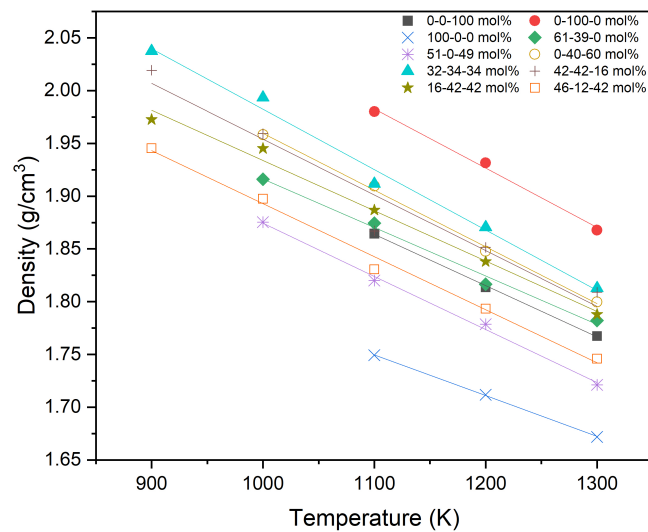


Figure 2: The density (g/cm^3) versus temperature (K) of all compositions studied (LiF-NaF-KF mol%).

145 The density can be analyzed by composition, as in fig. 3, where there is an overall decrease in
 146 the density as the percent of LiF increases. The opposite occurs in fig. 3b, where the density
 147 increases as the percent of NaF increases. Looking at fig. 3c, there appears to be little effect as
 148 the percent of KF changes. This seems to be reasonable, as the density of LiF is the lowest, the
 149 density of NaF is the highest, and the density of KF is at an intermediate value between the
 150 other two. It should be emphasized that in fig. 3, ternary, binary, and unary salt densities are
 all included. For the three temperatures at which all ten compositions were studied, ternary

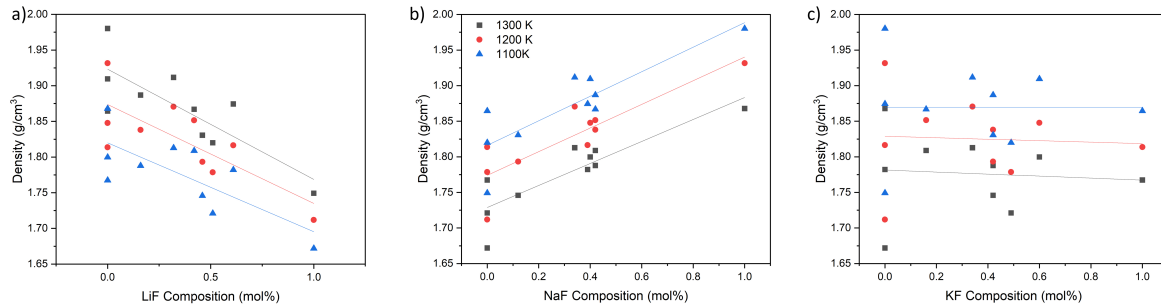


Figure 3: The density (g/cm^3) as a function of the composition of a) LiF (mol%), b) NaF (mol%), and c) KF (mol%) for different FLiNaK salts.

151 heatmaps, shown in fig. 4, were generated to better visualize the effects of the changing
 152 composition. While a limited number of compositions were utilized for the construction of the
 153 ternary density heat maps, they can clearly illustrate the dependence upon the composition.
 154 The composition of the mixture with respect to the LiF-NaF binary system is the primary
 155 determining factor for the density of the ternary, with the KF composition having nearly a
 156 negligible effect. It appears that density decreases more sharply as the composition nears LiF
 157 than the density decreases as the NaF composition increases, but additional data points at
 158 intermediate compositions would be required to verify these behaviors. For the four ternary
 159 phases, the eutectic is somewhat the outlier, possessing the least NaF and thus exhibiting
 160 the lowest density. The lower density of the eutectic composition compared to other ternary
 161 compositions may or may not be preferable. Regardless, these variations are somewhat minor.
 162 These conclusions hold across the temperature range studied. More complex density surfaces
 163 may be present but are not identifiable with the limited number of compositions studied here.

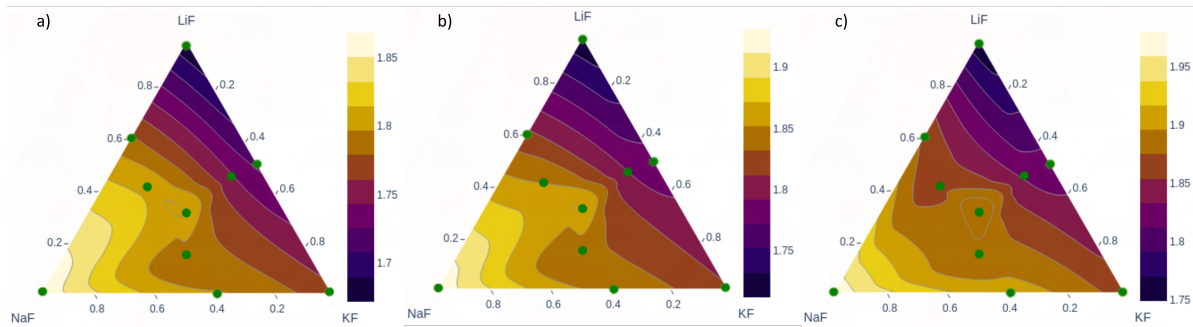


Figure 4: Ternary heatmap of the density (g/cm^3) of FLiNaK at a) 1300 K, b) 1200 K, and c) 1100 K.

165 Experimental densities are available for comparison with the eutectic composition. When
 166 compared to experimental values from Janz [29] (shown in fig. 5a), this work slightly under-
 167 predicts the density at all temperatures. The data deviates on average by 0.05 g/cc from
 168 Janz. For the individual salt endpoints (LiF, NaF, KF), the comparisons with experiments
 169 are shown in fig. 5b. There is a consistent, but minor, underprediction for the densities at all
 170 temperatures, but the change in the density with temperature shows good agreement, as the
 171 average deviation across all individual salts is 0.06 g/cc. As experimental measurements often
 172 report uncertainties on the order of 1-5% [30], there is general confidence in the magnitude
 173 and trends of the density with varying compositions.

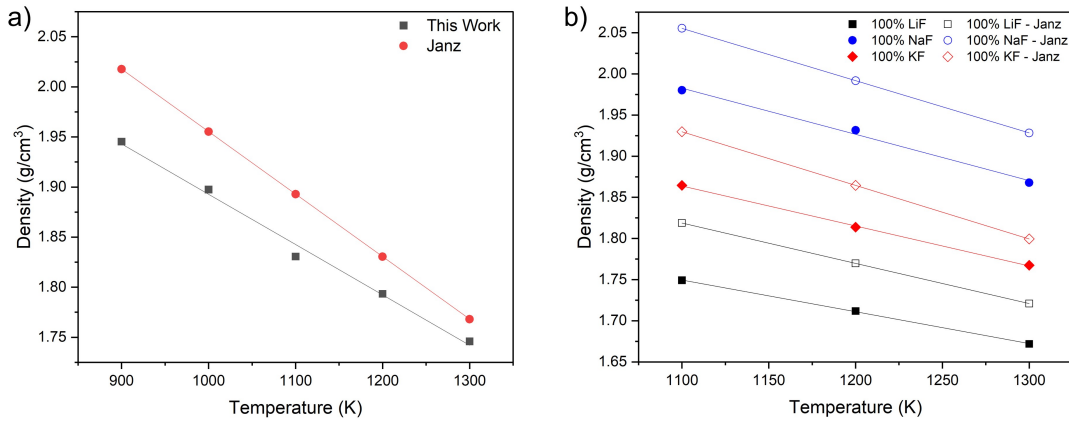


Figure 5: Comparison of density, g/cm^3 , versus temperature, K, of a) the eutectic composition with literature[29] and b) pure salts with literature[30].

174 The thermal expansion can be taken from the slope of the density in fig. 2 with respect
 175 to temperature (eq. (3)). The thermal expansion coefficient is plotted versus composition in
 176 fig. 6. The trends of the thermal expansion with respect to composition are not as strong as
 177 those for density. The LiF concentration in fig. 6a has a negative impact on the coefficient
 178 of thermal expansion. However, as shown in fig. 6b and fig. 6c, there is not a statistically
 179 significant impact on the thermal expansion of varying compositions of NaF or KF. However,
 180 with increasing NaF and KF, there is a minor increase in the thermal expansion. The
 181 minimum thermal expansion of the four ternary compositions occurs at 16-42-42 mol %, and
 182 the maximum occurs at 32-34-34 mol %. When considering only the ternary compositions,
 183 the previously stated trends do not apply as there is no statistically significant relationship
 184 between the composition of the unary salts and thermal expansion.

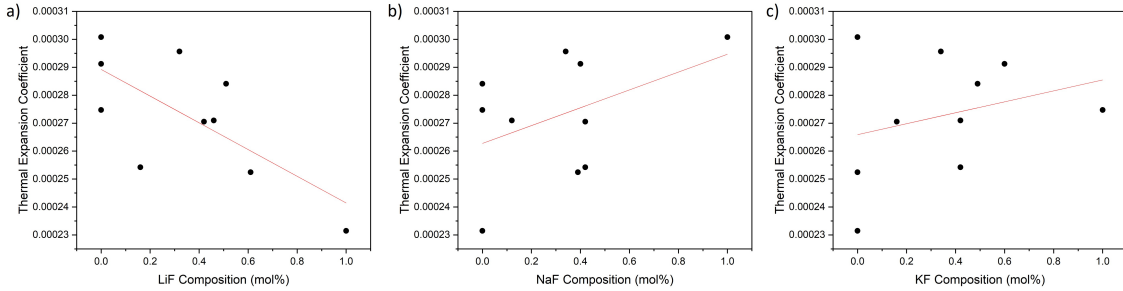


Figure 6: The thermal expansion coefficient versus the composition of a) LiF (mol%), b) KF (mol%), and c) NaF (mol%) for different FLiNaK salts.

185 3.2. Bulk Modulus and Compressibility

186 The bulk modulus and the compressibility are shown in fig. 7. It should be emphasized
 187 that the compressibility is the inverse of the bulk modulus. Both are shown here for com-
 188 pleteness. The degree of compressibility of a fluid has strong implications for its dynamics.
 189 As expected, the compressibility increases as the temperature increases. There is significant
 190 scatter in the data, which makes drawing specific conclusions regarding compositional de-
 191 pendence difficult, but generally, the eutectic composition has an intermediate value of the
 192 compressibility. The near equiatomic ternary salt has the lowest compressibility, and the
 193 low LiF content salt has the highest compressibility. Compared to two binary chloride salts
 194 (LiCl-KCl [24] and NaCl-MgCl₂ [31]), the ternary compositions of FLiNaK display a lower
 195 value of the compressibility. Only ternary salts are included here as non-ternary compo-
 196 sitions were analyzed in an NPT ensemble, which did not allow for the evaluation of the bulk
 197 modulus.

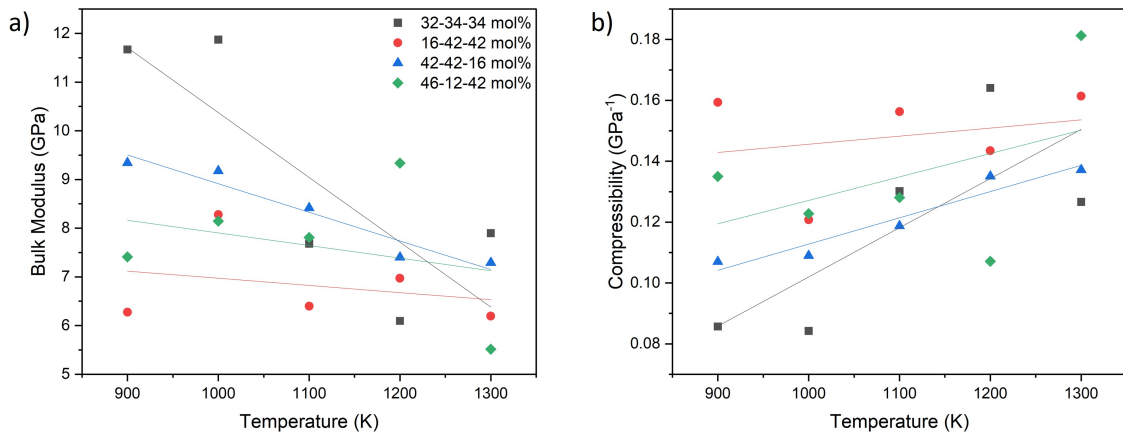


Figure 7: a) Bulk modulus and b) compressibility of the four ternary compositions versus temperature

198 3.3. Heat Capacity and Enthalpy of Mixing

199 Heat capacity is a required parameter for thermal hydraulics models describing heat trans-
200 port in molten salt systems[3]. The heat capacity for FLiNaK is best visualized as a ternary
201 heatmap, shown in fig. 8. The heat capacity is greatest around the middle compositions
202 and decreases as the system moves towards the three pure alkali-halide salt constituents. As
203 stated, the exact contour locations may vary from their depiction here due to the limited
204 number of ternary compositions, but the variance in the heat capacity with composition,
205 in that a near equiatomic mixture has the highest heat capacity, is quite consistent. The
206 total energy from AIMD simulations shows a linear dependence, thus the heat capacity is
207 effectively constant over the investigated temperature range. Williams et al. report the heat
208 capacity of the eutectic composition to be 77.9 J/mol-K at 973 K[32], which compares quite
209 favorably to the calculated value of 67.6 J/mol-K from this work. Compared to the reported
210 literature value, this work underpredicts the heat capacity by 13.2%, but is neglecting the
211 electronic contribution to the heat capacity, which, if included, would decrease the discrep-
212 ancies. It should be noted that heat capacity measurements are notoriously difficult in molten
213 salts, and often are in disagreement with one another [33]. Generally, a higher heat capacity
214 is preferable for thermal hydraulics applications, and thus this work points to a potential
215 benefit of utilizing near-equiatomic compositions of FLiNaK.

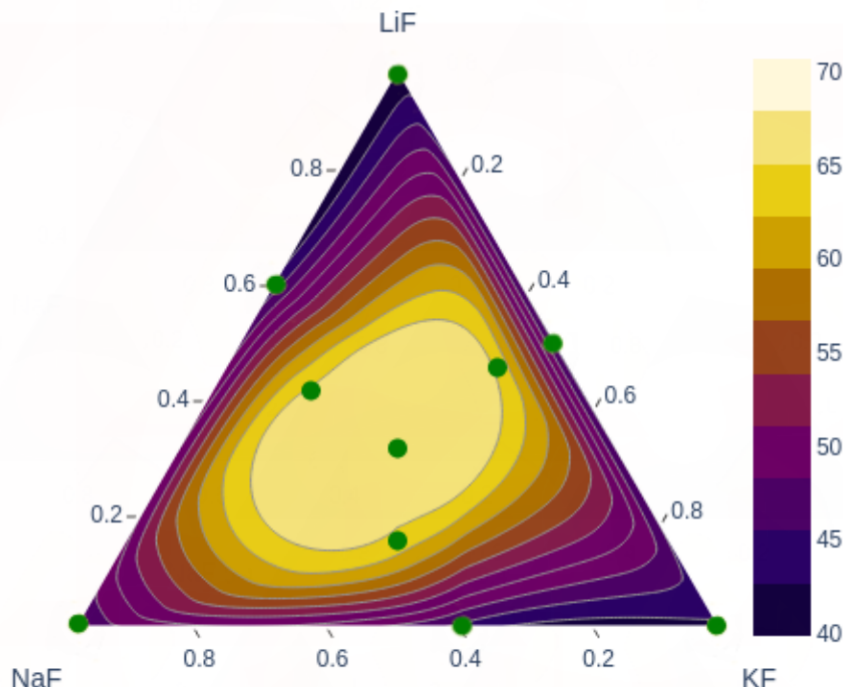


Figure 8: Ternary heatmap of the heat capacity of FLiNaK (J/mol-K).

216 The enthalpy of mixing is plotted against each of the pure alkali-halide salt constituents
217 in fig. 9. Considering that this figure includes both ternary and binary compounds, the char-
218 acteristic inverse hull shape is not present. However, intermediate compositions display the
219 lowest enthalpy of mixing, with the near-equiatomic (32-34-34) composition exhibiting the

global lowest energy. Including entropic effects to yield a free energy of formation was beyond the scope of this work, but it is anticipated that the near equiatomic composition would likely display the largest entropy, and thus the lowest free energy. Unfortunately, there is no experimental data for comparison. Additionally, prior computational investigations were typically restricted to the eutectic composition and did not explore the unary salt components, which prevented them from determining the enthalpy of formation. Experimental and additional computational studies are warranted to validate these results.

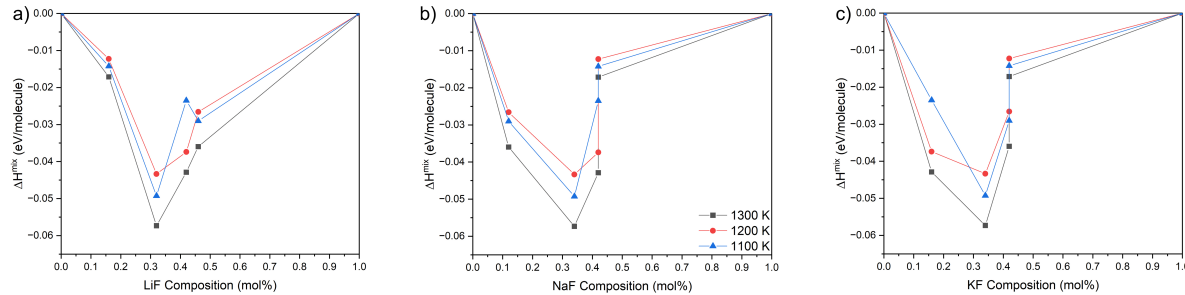


Figure 9: Graph of the enthalpy of mixing, eV/molecule, versus composition of a) LiF (mol%), b) NaF (mol%), and c) KF (mol%).

3.4. Coordination Analysis

The local atomic structure is analyzed by means of the radial pair distribution function (RDF). The RDF, or $g(r)$, measures the probability of finding a particle at distance r given that there is a particle at position $r = 0$. The peak of the RDF for each pair is the most probable location of the first-nearest-neighbor (1nn). The RDF for eutectic LiF-NaF-KF is shown in fig. 10 at 900 K. Note that not all pair-wise interactions are shown in fig. 10, to aid in readability. Also, this RDF constitutes a time average over 3 ps of a given simulation at the zero-pressure volume at 900 K. The 1nn distance is then determined and compared to an x-ray diffraction study conducted at 793 K in table 1. Generally, the RDF compares very favorably to the experimental results, as well as a prior computational study [6]. The most significant difference being for the F-F peak, which is overestimated by approximately 0.09 Å. However, the experimental results assumed a Gaussian distribution for their analysis, which may induce small errors, and reported a mean square-root displacement of 0.41 Å, indicating a broad peak, which is in accordance with these results and provides additional confidence in the accuracy of the simulations. The RDFs of the other ternary systems were analyzed to identify potential variations with somewhat minor compositional differences. The individual pair distances did not statistically change for the primary species, however, the F-F bond did show some variance depending upon the system, with the low Li concentration (16-42-42) displaying the longest F-F 1nn distance (3.33 Å) and the eutectic displaying the shortest F-F bond 1nn distance (3.14 Å) (table A.3). There is not a clear correlation between F-F 1nn distance and density, which one might expect. However, there is a negative linear correlation ($R^2=0.98$) with the Li content, with greater Li content exhibiting shorter F-F 1nn distances. These minor structural variations would need to be confirmed via experiments and may provide insight into dynamical properties related to the distribution of F atoms in FLiNaK salts.

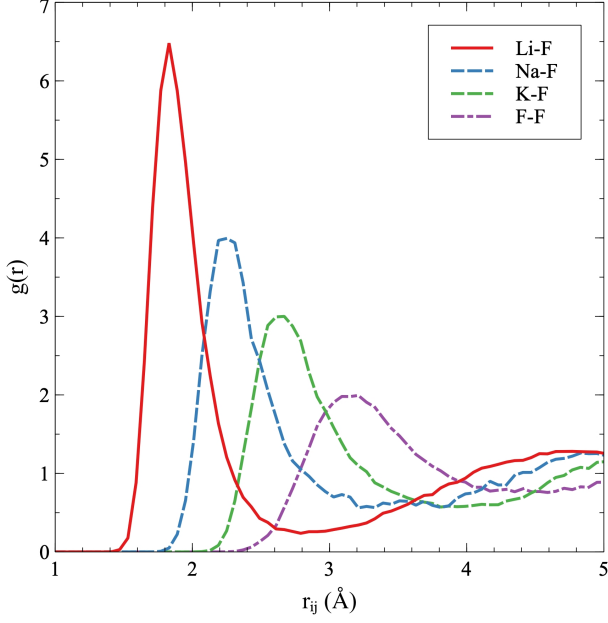


Figure 10: Partial radial distribution functions for eutectic LiF-NaF-KF at 900 K.

Table 1: First nearest neighbor distances for eutectic LiF-NaF-KF at 900 K. Results are compared against experiment at 793 K [34].

Pair	r_{ij} (Å)	r_{ij} (Å) [34]
Li-F	1.82	1.83
Na-F	2.23	2.18
K-F	2.64	2.59
F-F	3.14	3.05

252 4. Conclusion

253 To characterize the thermophysical properties of FLiNaK, a first principles computa-
 254 tional investigation was performed for four ternary compositions, three binary eutectic com-
 255 positions, and three pure alkali-halide salt constituents. The computational results of the
 256 density slightly underpredicted the experimental values at all temperatures for the eutectic
 257 and pure salt compositions. However, generally good agreement is observed. The density
 258 is positively correlated with the NaF concentration and negatively correlated with the LiF
 259 concentration. The thermal expansion was determined to decrease with increasing LiF con-
 260 centration, but there was no statistically significant dependence on NaF or KF. The large
 261 scatter in the data for the bulk modulus and compressibility resulted in an inability to draw
 262 specific conclusions about compositional dependence, however, the compressibility increased
 263 with the temperature, as expected, and displays a magnitude lower than comparable chloride
 264 salts. The results for the heat capacity, like the density, underpredicted the literature value,
 265 but are likely within experimental uncertainties. In the enthalpy of mixing versus composi-
 266 tion, the ternary compositions display the lowest formation energy, with the near equiatomic
 267 composition possessing the minimum.

268 As the interest in molten salt reactors is renewed, there is a need for thermophysical

269 properties of salt systems at varied compositions rather than just the eutectic composition.
270 Currently, these properties are largely unknown, but can be elucidated through first principles
271 methods. This work has shown that some thermophysical properties can exhibit significant
272 differences with relatively minor compositional variance, indicating the potential for tailoring
273 even well-known molten salt systems to target specific property behaviors. Further exper-
274 imental work is necessary to validate the results presented in this manuscript, providing
275 further confidence in the ability of first principles methods to explore the vast composition
276 and temperature space relevant to molten salts in nuclear applications.

277 **5. Acknowledgements**

278 This work was supported through the NC State Nuclear Engineering Undergraduate Re-
279 search Scholar Program with funding courtesy of the College of Engineering Enhancement
280 Fee. This work is also supported through the INL Laboratory Directed Research and Develop-
281 ment (LDRD) Program under DOE Idaho Operations Office Contract DE-AC07-05ID14517.
282 This research made use of the resources of the High-Performance Computing Center at Idaho
283 National Laboratory, which is supported by the Office of Nuclear Energy of the U.S. Depart-
284 ment of Energy and the Nuclear Science User Facilities.

285 **Appendix A.**

Table A.1: The density (g/cm³) of LiF-NaF-KF at different temperatures.

Composition (LiF-NaF-KF)	900 K	1000 K	1100 K	1200 K	1300 K
eutectic 46-12-42	1.95	1.90	1.83	1.79	1.75
16-42-42	1.97	1.95	1.89	1.84	1.79
32-34-34	2.04	1.99	1.91	1.87	1.81
42-42-16	2.02	1.96	1.87	1.85	1.81
0-40-60	-	1.96	1.91	1.85	1.80
51-0-49	-	1.88	1.82	1.78	1.72
61-39-0	-	1.92	1.87	1.82	1.78
100-0-0	-	-	1.75	1.71	1.67
0-100-0	-	-	1.98	1.93	1.87
0-0-100	-	-	1.86	1.81	1.77

Table A.2: The coefficient of thermal expansion (α), compressibility (β at 1100 K), heat capacity (C_P), and enthalpy of mixing (ΔH_{mix} at 1300 K) of LiF-NaF-KF.

Composition (LiF-NaF-KF)	$\alpha \times 10^{-4}$	β (GPa $^{-1}$)	C_P (J/mol-K)	ΔH_{mix} (eV/molecule)
eutectic 46-12-42	2.88	0.128	67.6	-0.027
16-42-42	2.66	0.121	66.8	-0.017
32-34-34	3.15	0.130	70.7	-0.057
42-42-16	2.93	0.119	68.3	-0.043
0-40-60	2.91	-	43.1	-0.007
51-0-49	2.84	-	43.0	-0.043
61-39-0	2.52	-	42.0	-0.028
100-0-0	2.31	-	39.9	-
0-100-0	3.01	-	44.4	-
0-0-100	2.75	-	41.9	-

Table A.3: The first-nearest-neighbor distances of the ternary LiF-NaF-KF salts at 900K.

Composition (LiF-NaF-KF)	F-F 1nn distance (Å)
eutectic 46-12-42	3.14
16-42-42	3.33
32-34-34	3.21
42-42-16	3.15

286 References

- [1] T. Porter, M. Vaka, P. Steenblik, D. Della Corte, Computational methods to simulate molten salt thermophysical properties, Commun Chem 5 (2022) 69. doi:10.1038/s42004-022-00684-6.
URL <https://www.nature.com/articles/s42004-022-00684-6>
- [2] G. Locatelli, M. Mancini, N. Todeschini, Generation iv nuclear reactors: Current status and future prospects, Energy Policy 61 (2013) 1503–1520. doi:10.1016/j.enpol.2013.06.101.
URL <https://www.sciencedirect.com/science/article/pii/S0301421513006083>
- [3] Freile, Ramiro, Kimber, Mark, Influence of molten salt-(flinak) thermophysical properties on a heated tube using cfd rans turbulence modeling of an experimental testbed, EPJ Nuclear Sci. Technol. 5 (2019) 16. doi:10.1051/epjn/2019027.
URL <https://doi.org/10.1051/epjn/2019027>
- [4] O. Beneš, R. Konings, Thermodynamic properties and phase diagrams of fluoride salts for nuclear applications, Journal of Fluorine Chemistry (2009) 22–29doi:<https://doi.org/10.1016/j.jfluchem.2008.07.014>.
URL <https://www.sciencedirect.com/science/article/pii/S0022113908002030>
- [5] J. Ambrosek, M. Anderson, K. Sridharan, T. Allen, Current status of knowledge of the fluoride salt (flinak) heat transfer, Nuclear Technology 165 (2009) 166–173.

- 305 doi:10.13182/NT165-166.
306 URL <https://www.tandfonline.com/doi/full/10.13182/NT165-166>
- 307 [6] B. A. Frandsen, S. D. Nickerson, A. D. Clark, A. Solano, R. Baral, J. Williams, J. Neue-
308 feind, M. Memmott, The structure of molten flinak, Journal of Nuclear Materials 537
309 (2020) 152219. doi:10.1016/j.jnucmat.2020.152219.
310 URL <https://www.sciencedirect.com/science/article/pii/S0022311520304736>
- 311 [7] M. Anderson, K. Sridharan, D. Morgan, P. Peterson, P. Calderoni, R. Scheele,
312 A. Casekka, B. McNamara, Heat transfer salts for nuclear reactor systems - chemistry
313 control, corrosion mitigation, and modeling, Tech. Rep. Project No. 10-905, University
314 of Wisconsin, Madison (1 2015). doi:10.2172/1169921.
315 URL <https://www.osti.gov/biblio/1169921>
- 316 [8] X. Liu, Y. Li, B. Wang, C. Wang, Raman and density functional theory stud-
317 ies of lutecium fluoride and oxyfluoride structures in molten flinak, Spectrochim-
318 ica Acta Part A: Molecular and Biomolecular Spectroscopy 251 (2021) 119435.
319 doi:10.1016/j.saa.2021.1194358.
320 URL <https://www.sciencedirect.com/science/article/pii/S1386142521000111>
- 321 [9] H. W. Hoffman, J. Lones, Fused salt heat transfer. part ii. forced convection heat trans-
322 fer in circular tubes containing naf-kf-lif eutectic, Tech. Rep. ORNL-1777, Oak Ridge
323 National Laboratory (2 1955). doi:10.2172/4016896.
324 URL <https://www.osti.gov/biblio/4016896>
- 325 [10] D. Holcomb, S. Cetiner, An overview of liquid-fluoride-salt heat transport sys-
326 tems, Tech. Rep. ORNL/TM-2010/156, Oak Ridge National Laboratory (10 2010).
327 doi:10.2172/990239.
- 328 [11] G. L. Yoder, Jr, D. W. Heatherly, D. F. Williams, Y. M. Elkassabgi, J. Caja, M. Caja,
329 J. Jordan, R. Salinas, Liquid fluoride salt experimentation using a small natural circu-
330 lation cell, Tech. Rep. ORNL/TM-2014/56, Oak Ridge National Laboratory (4 2014).
331 doi:10.2172/1130418.
332 URL <https://www.osti.gov/biblio/1130418>
- 333 [12] M. Salanne, C. Simon, P. Turq, P. A. Madden, Heat-transport properties of molten
334 fluorides: Determination from first-principles, Journal of Fluorine Chemistry 130 (2009)
335 38–44. doi:10.1016/j.jfluchem.2008.07.013.
- 336 [13] S.-C. Lee, Y. Zhai, Z. Li, N. P. Walter, M. Rose, B. J. Heuser, Y. Z, Comparative
337 studies of the structural and transport properties of molten salt flinak using the machine-
338 learned neural network and reparametrized classical forcefields, The Journal of Physical
339 Chemistry B 125 (2021) 10562–10570. doi:10.1021/acs.jpcb.1c05608.
340 URL <https://pubs.acs.org/doi/10.1021/acs.jpcb.1c05608>
- 341 [14] C. Sona, M. A. Khanwale, C. S. Mathpati, A. Borgohain, N. K. Maheshwari, In-
342 vestigation of flow and heat characteristics and structure identification of flinak

- 343 in pipe using cfd simulations, Applied Thermal Engineering 70 (2014) 451–461.
344 doi:10.1016/j.applthermaleng.2014.05.043.
- 345 [15] H. Nam, A. Bengtson, K. Vörtler, S. Saha, R. Sakidja, D. Morgan, First-principles
346 molecular dynamics modeling of the molten fluoride salt with cr solute, Journal of Nu-
347 clear Materials 449 (2014) 148–157. doi:10.1016/j.jnucmat.2014.03.014.
348 URL <https://www.sciencedirect.com/science/article/pii/S0022311514001238>
- 349 [16] A. D. Clark, W. L. Lee, A. R. Solano, T. B. Williams, G. S. Meyer, G. J. Tait,
350 B. C. Battraw, S. D. Nickerson, Complexation of mo in flinak molten salt: Insight
351 from ab initio molecular dynamics, Journal of Physical Chemistry B 125 (2020).
352 doi:10.1021/acs.jpcb.0c07354.
- 353 [17] D. Sprouster, G. Zheng, S.-C. Lee, D. Olds, C. Agca, J. McFarlane, Y. Z, B. Khaykovich,
354 Molecular structure and phase equilibria of molten fluoride salt with and without
355 dissolved cesium: Flinak–csf (5 mol %), ACS Applied Energy Materials 5 (2022).
356 doi:10.1021/acsadm.2c00544.
- 357 [18] L. Martínez, R. Andrade, E. G. Birgin, J. M. Martínez, Packmol: A
358 package for building initial configurations for molecular dynamics sim-
359 ulations, Journal of Computational Chemistry 30 (13) (2009) 2157–
360 2164. arXiv:<https://onlinelibrary.wiley.com/doi/pdf/10.1002/jcc.21224>,
361 doi:<https://doi.org/10.1002/jcc.21224>.
362 URL <https://onlinelibrary.wiley.com/doi/abs/10.1002/jcc.21224>
- 363 [19] A. Bengtson, H. O. Nam, S. Saha, R. Sakidja, D. Morgan, First-principles molecular
364 dynamics modeling of the licl–kcl molten salt system, Computational Materials Science
365 83 (2014). doi:10.1016/j.commatsci.2013.10.043.
366 URL <https://www.sciencedirect.com/science/article/pii/S0927025613006630>
- 367 [20] D. Andersson, B. Beeler, Ab initio molecular dynamics (aimd) simulations of
368 nacl, ucl3 and nacl-ucl3 molten salts, Journal of Nuclear Materials 568 (2022).
369 doi:10.1016/j.jnucmat.2022.153836.
370 URL <https://www.sciencedirect.com/science/article/pii/S0022311522003221>
- 371 [21] G. Kresse, J. Hafner, Ab initio molecular dynamics for liquid metals, Phys. Rev. B 47
372 (1993) 558–561. doi:10.1103/PhysRevB.47.558.
373 URL <https://link.aps.org/doi/10.1103/PhysRevB.47.558>
- 374 [22] G. Kresse, J. Furthmüller, Efficiency of ab-initio total energy calculations for metals and
375 semiconductors using a plane-wave basis set, Computational Materials Science 6 (1996)
376 15–50. doi:[https://doi.org/10.1016/0927-0256\(96\)00008-0](https://doi.org/10.1016/0927-0256(96)00008-0).
377 URL <https://www.sciencedirect.com/science/article/pii/0927025696000080>
- 378 [23] G. Kresse, J. Furthmüller, Efficient iterative schemes for ab initio total-energy
379 calculations using a plane-wave basis set, Phys. Rev. B 54 (1996) 11169–11186.
380 doi:10.1103/PhysRevB.54.11169.
381 URL <https://link.aps.org/doi/10.1103/PhysRevB.54.11169>

- [24] K. Duemmler, Y. Lin, M. Woods, T. Karlsson, R. Gakhar, B. Beeler, Evaluation of thermophysical properties of the licl-kcl system via ab initio and experimental methods, Journal of Nuclear Materials 559 (2022) 153414. doi:<https://doi.org/10.1016/j.jnucmat.2021.153414>.
URL <https://www.sciencedirect.com/science/article/pii/S0022311521006346>
- [25] J. Klimeš, D. R. Bowler, A. Michaelides, Chemical accuracy for the van der waals density functional, Journal of Physics: Condensed Matter 22 (2) (2009) 022201. doi:[10.1088/0953-8984/22/2/022201](https://doi.org/10.1088/0953-8984/22/2/022201).
- [26] J. Klimeš, D. R. Bowler, A. Michaelides, Van der waals density functionals applied to solids, Physical Review B 83 (19) (may 2011). doi:[10.1103/physrevb.83.195131](https://doi.org/10.1103/physrevb.83.195131).
URL <https://doi.org/10.1103%2Fphysrevb.83.195131>
- [27] S. Grimme, J. Antony, S. Ehrlich, H. Krieg, A consistent and accurate ab initio parametrization of density functional dispersion correction (dft-d) for the 94 elements h-pu, The Journal of Chemical Physics 132 (15) (2010) 154104. arXiv:<https://doi.org/10.1063/1.3382344>, doi:[10.1063/1.3382344](https://doi.org/10.1063/1.3382344).
URL <https://doi.org/10.1063/1.3382344>
- [28] A. Stukowski, Visualization and analysis of atomistic simulation data with OVITO-the Open Visualization Tool, MODELLING AND SIMULATION IN MATERIALS SCIENCE AND ENGINEERING 18 (1) (JAN 2010). doi:[10.1088/0965-0393/18/1/015012](https://doi.org/10.1088/0965-0393/18/1/015012).
- [29] G. Janz, R. Tomkins, Physical properties data compilations relevant to energy storage. iv. molten salts: Data on additional single and multi-component salt systems, Tech. Rep. NSRDS-NBS 61, National Bureau of Standards (1981).
- [30] G. Janz, Thermodynamic and transport properties for molten salts: Correlation equations for critically evaluated density, surface tension, electrical conductance, and viscosity data, Journal of Physical and Chemical Reference Data 17 (1988).
- [31] K. Duemmler, M. Woods, T. Karlsson, R. Gakhar, B. Beeler, An ab initio molecular dynamics investigation of the thermophysical properties of molten nacl-mgcl₂, Journal of Nuclear Materials 570 (2022) 153916. doi:<https://doi.org/10.1016/j.jnucmat.2022.153916>.
URL <https://www.sciencedirect.com/science/article/pii/S0022311522004020>
- [32] D. F. Williams, Assessment of candidate molten salt coolants for the advanced high temperature reactor (ahtr), Tech. Rep. ORNL/TM-2006/12, Oak Ridge National Laboratory (3 2006). doi:[10.2172/885975](https://doi.org/10.2172/885975).
URL <https://www.osti.gov/biblio/885975>
- [33] S. G. Robertson, R. Wiser, W. Yang, D. Kang, S. Choi, E. Baglietto, M. P. Short, The curious temperature dependence of fluoride molten salt thermal conductivity, Journal of Applied Physics 131 (22), 225102 (06 2022). arXiv:https://pubs.aip.org/aip/jap/article-pdf/doi/10.1063/5.0088059/16508374/225102_1_online.pdf, doi:[10.1063/5.0088059](https://doi.org/10.1063/5.0088059).
URL <https://doi.org/10.1063/5.0088059>

- ⁴²¹ [34] K. Igarashi, Y. Okamoto, J. Mochinaga, H. Ohno, X-ray diffraction study of molten
⁴²² eutectic lif–naf–kf mixture, J. Chem. Soc., Faraday Trans. 1 84 (1988) 4407–4415.
⁴²³ doi:10.1039/F19888404407.
- ⁴²⁴ URL <http://dx.doi.org/10.1039/F19888404407>